Supporting Information

Spatial Construction of Pd and MnO_x on Facet-engineered $BiVO_4$ Photocatalyst for Efficient Removal of Glyphosate Pesticide

Nengcong Yang[1,#], Lulu Liu[1,#], Yue Chen[1,#], Mengmeng Liu[1], Zhian Chen[1], Ruyan Hou[1,*], Sheng Ye[1,*], Rengui Li[2,*]

[1] State Key Laboratory of Tea Plant Germplasm Innovation and Resource Utilization, Agricultural Photocatalysis Laboratory, School of Materials and Chemistry, Anhui Agricultural University, Hefei 230036, China

[2] State Key Laboratory of Catalysis, Dalian National Laboratory for Clean Energy, Dalian Institute of Chemical Physics, Chinese Academy of Sciences, Dalian 116023, P. R. China

*Corresponding author

E-mail: hry@ahau.edu.cn; sye503@ahau.edu.cn; rgli@dicp.ac.cn

[#] These authors contributed equally: Nengcong Yang, Lulu Liu, Yue Chen

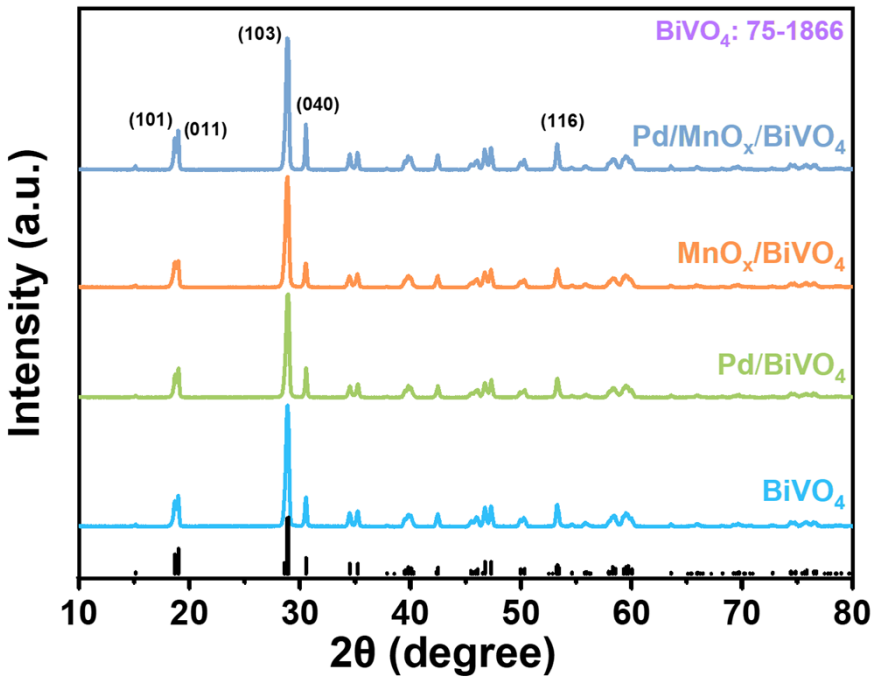

Fig. S1. XRD patterns of decahedron $BiVO_4$ crystals and $BiVO_4$ with different cocatalysts.

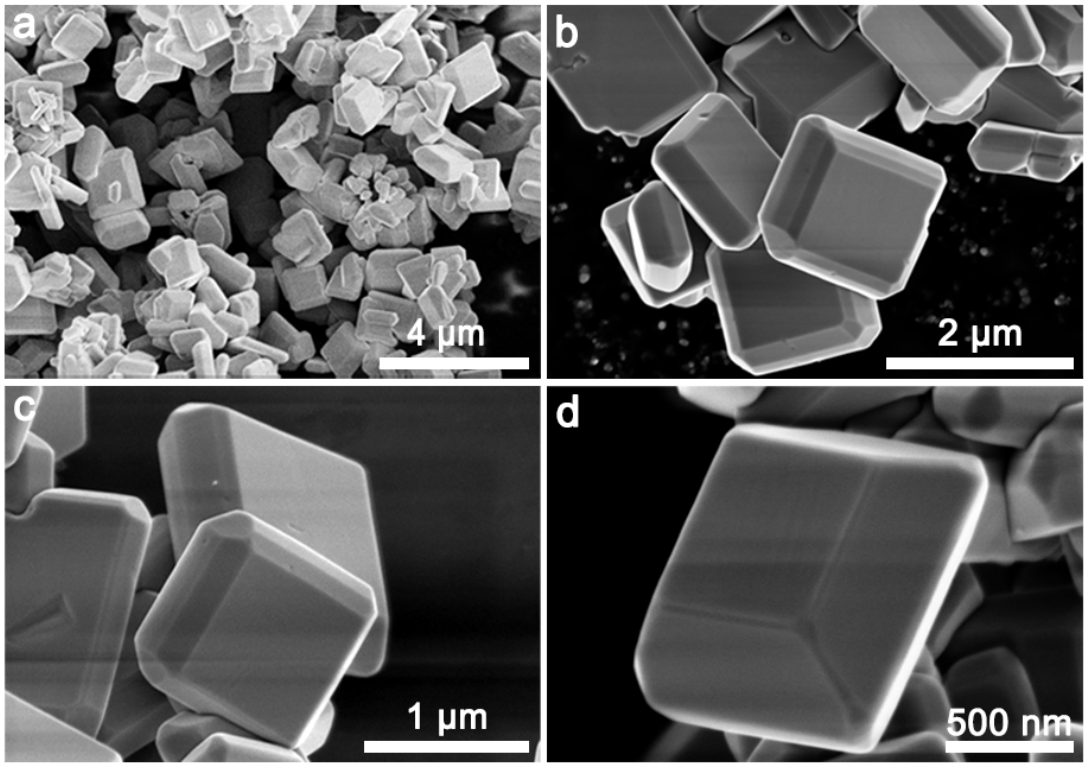

Fig. S2. SEM images of $BiVO_4$ nanoparticles.

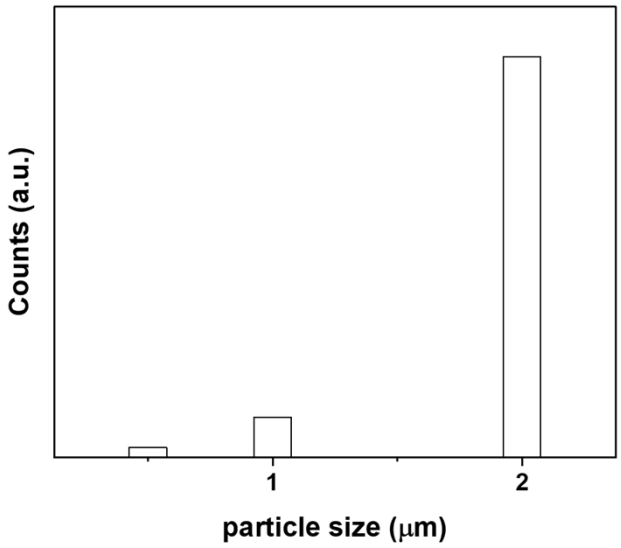

Fig. S3. The particle size distribution of $BiVO_4$ particles.

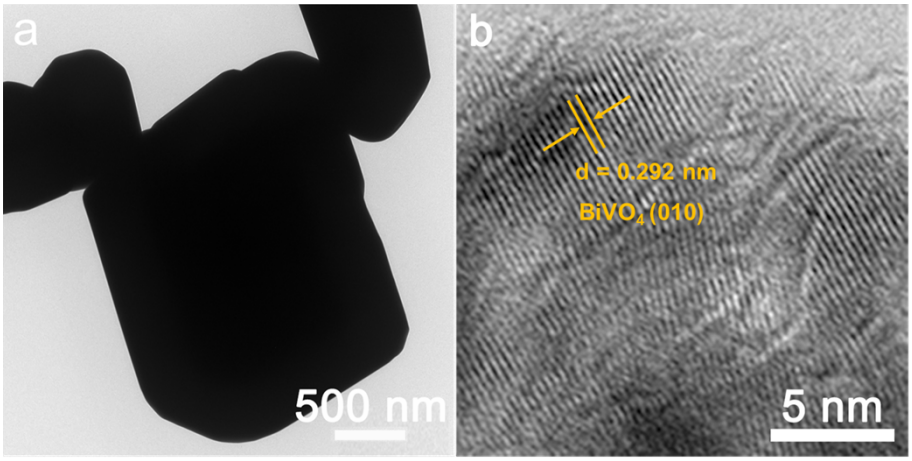

Fig. S4. TEM and HRTEM images of $BiVO_4$ nanoparticle.

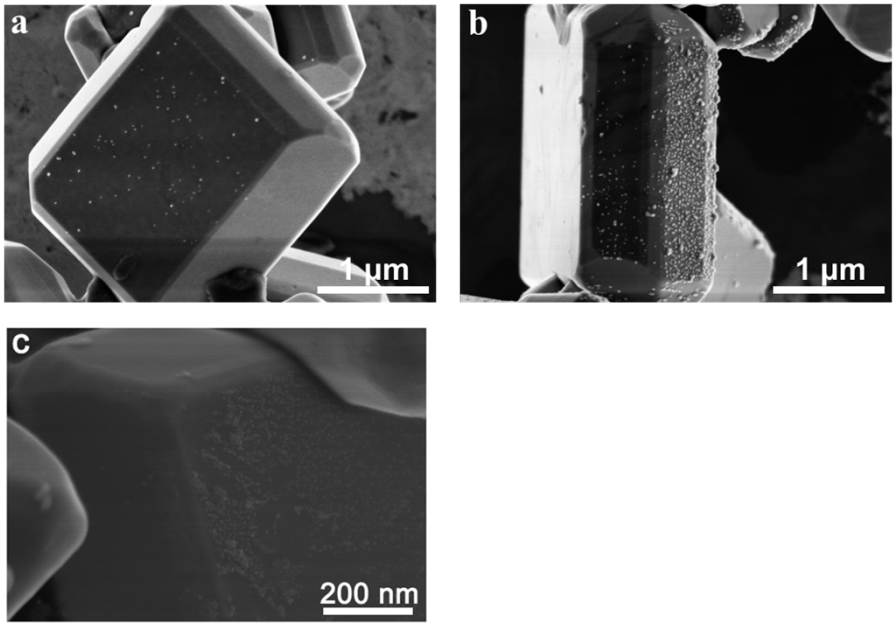

Fig. S5. SEM images of $BiVO_4$ samples with deposition of (a) Au, (b) Ag, (c) Pd.

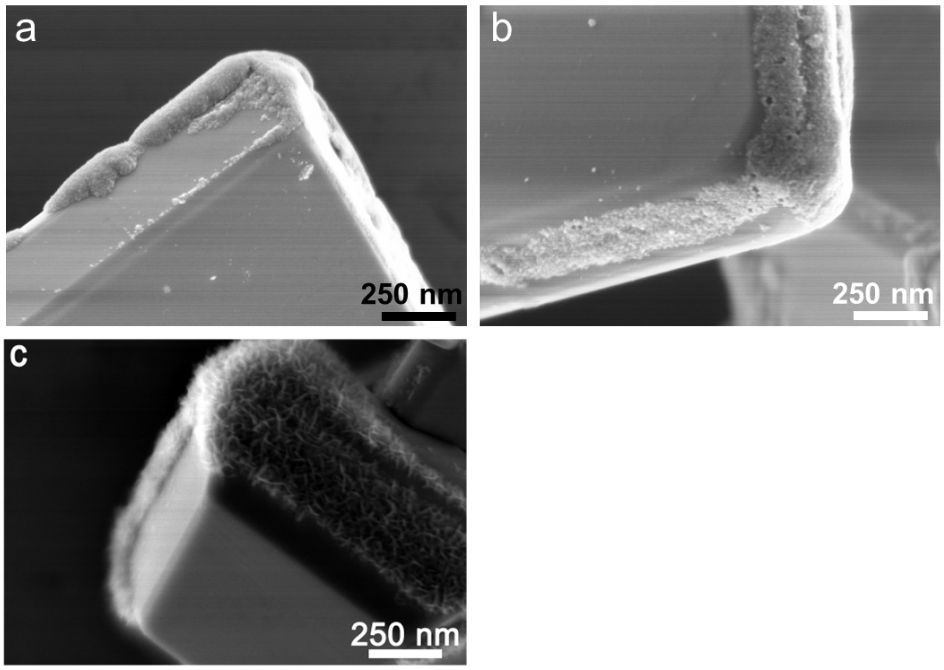

Fig. S6. SEM images of $BiVO_4$ samples with oxide deposition of (a) CoO_x, (b) NiO_x, (c) MnO_x.

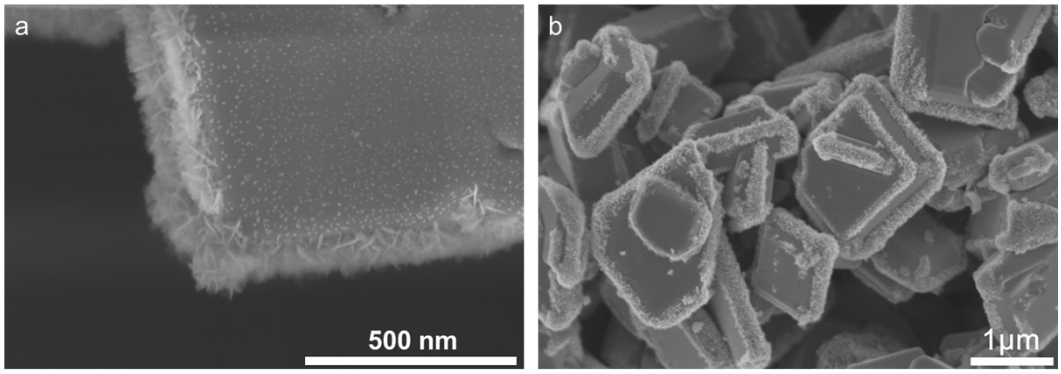

Fig. S7. SEM images of $BiVO_4$ samples with selective deposition of dual cocatalysts.

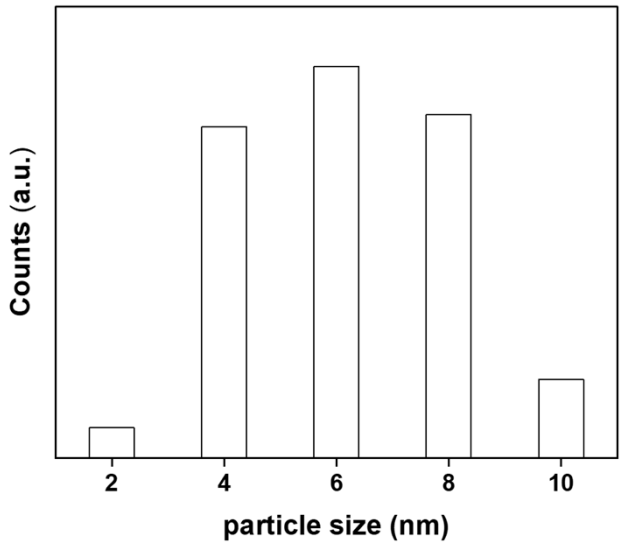

Fig. S8. The particle size distribution of Pd nanoparticles on $Pd/MnO_x/BiVO_4$.

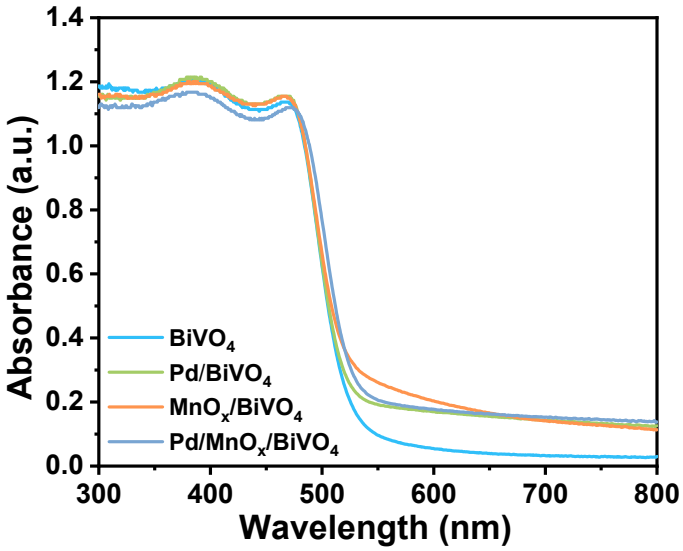

Fig. S9. UV-vis diffuse reflectance spectra of decahedron $BiVO_4$ crystals and $BiVO_4$ with different cocatalysts.

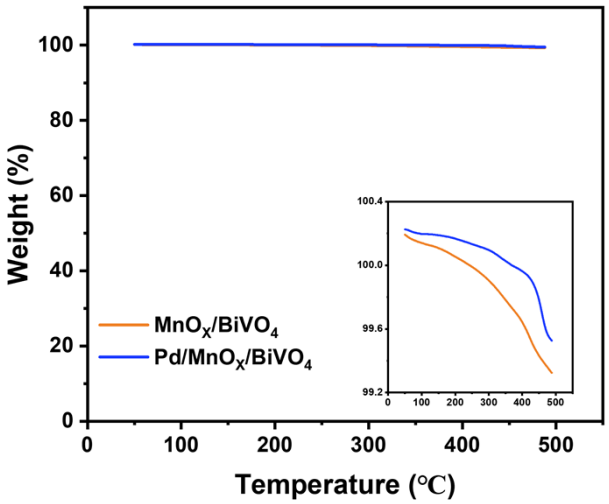

Fig. S10. Thermogravimetry curves of $MnO_x/BiVO_4$ and $Pd/MnO_x/BiVO_4$.

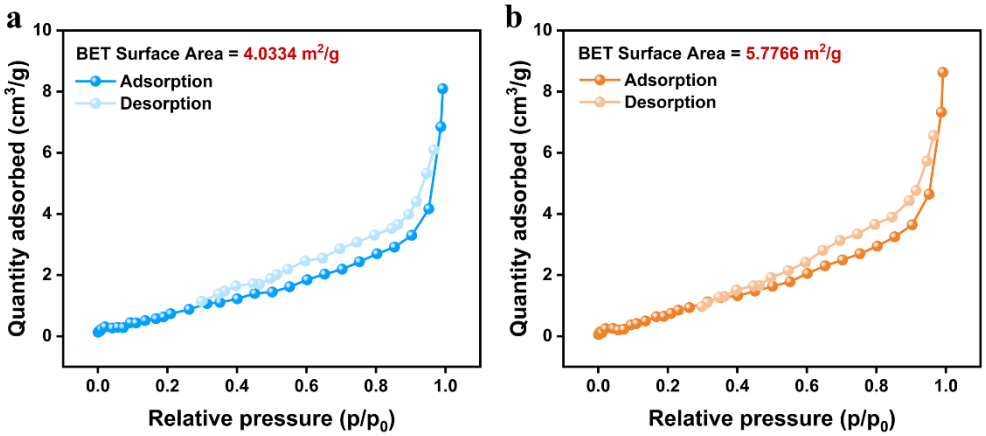

Fig. S11. BET measurement of $MnO_x/BiVO_4$ and $Pd/MnO_x/BiVO_4$.

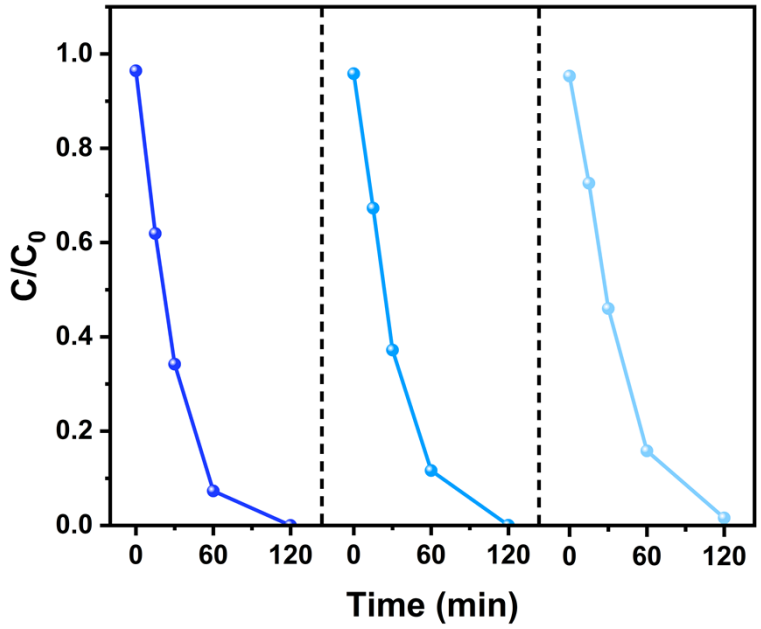

Fig. S12. The stability tests of 3 cycles for $Pd/MnO_x/BiVO_4$.

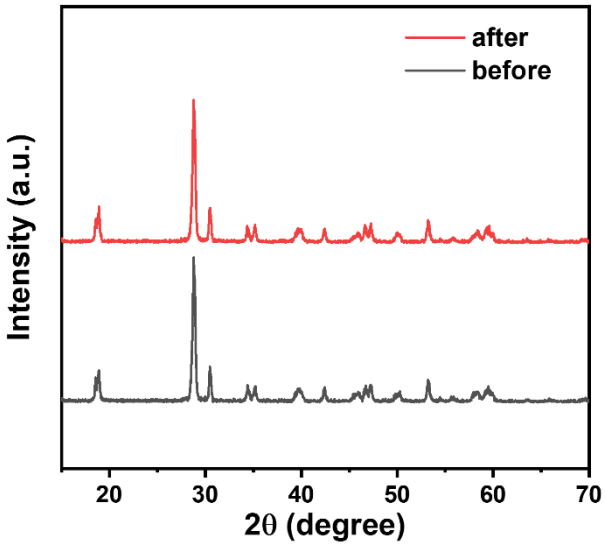

Fig. S13. XRD pattern of $Pd/MnO_x/BiVO_4$ photocatalyst before and after degradation.

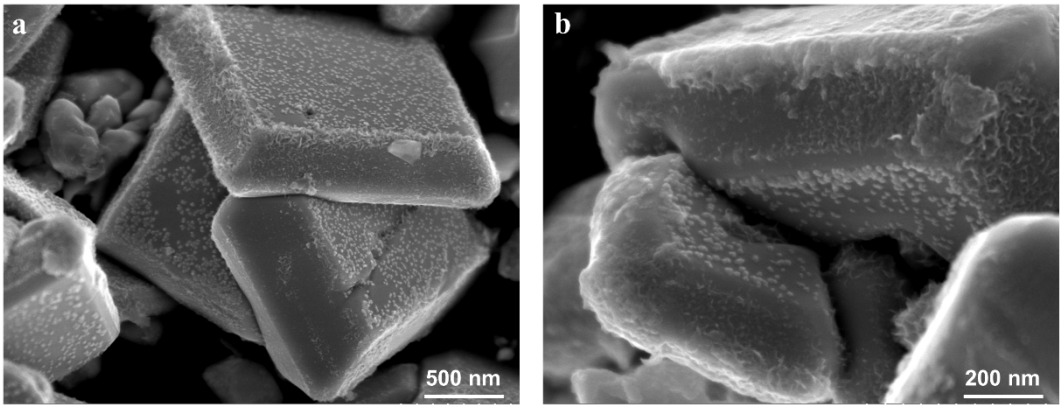

Fig. S14. SEM images of $Pd/MnO_x/BiVO_4$ photocatalyst after degradation.

Table S1. The concentration of Pd and Mn elements in the reaction solution

Element	Sample	Concentrations (ppm)
Pd	Before reaction	0
	After reaction	0.238
Mn	Before reaction	0
	After reaction	0.317

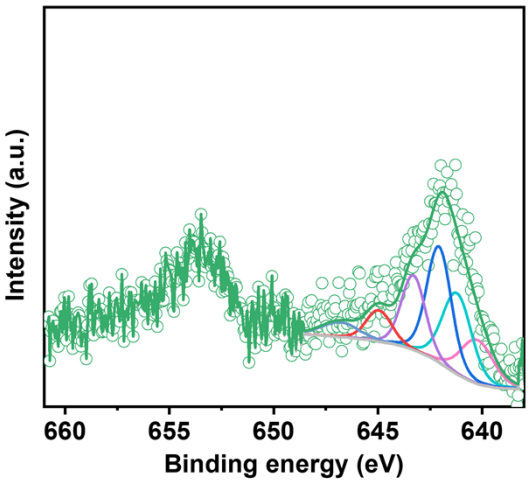

Fig. S15. Corresponding XPS fine spectra of $MnO_x/BiVO_4$ of Mn 2p.

Table S2. The summarized fitting parameters of Mn $2p_{3/2}$

Sample	Element	$2p_{3/2}$ Position (eV)	Area ratio (%)
$MnO_x/BiVO_4$-before	Mn^{3+}	640.25	14.61
		641.21	24.08
		643.30	18.31
	Mn^{4+}	642.07	29.23
		644.95	8.14
		646.81	5.63
$MnO_x/BiVO_4$-after	Mn^{3+}	640.22	10.24
		641.12	22.21
		643.19	19.11
	Mn^{4+}	642.19	32.40
		644.15	8.32
		646.05	7.71

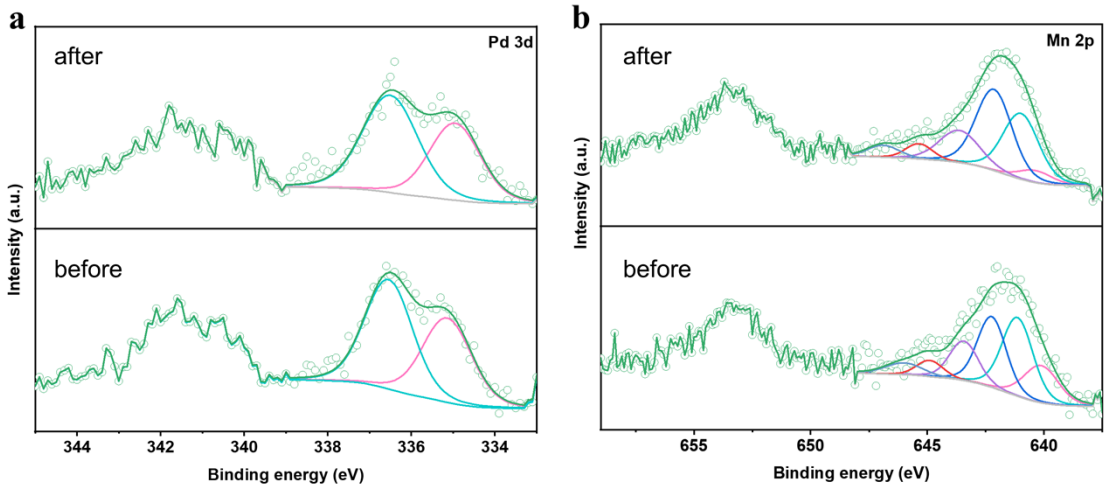

Fig. S16. Corresponding XPS fine spectra of $Pd/MnO_x/BiVO_4$: (a) Pd 3d and (b) Mn 2p.

Table S3. The summarized fitting parameters of Pd $3d_{5/2}$

Sample		Element	$3d_{5/2}$ Position (eV)	Area ratio (%)
$Pd/MnO_x/BiVO_4$-before		Pd	335.14	44.13
		Pd^{2+}	336.54	55.87
$Pd/MnO_x/BiVO_4$-after		Pd	335.16	42.21
		Pd^{2+}	336.50	57.79

Table S4. The summarized fitting parameters of Mn $2p_{3/2}$

Sample	Element	$2p_{3/2}$ Position (eV)	Area ratio (%)
$Pd/MnO_x/BiVO_4$-before	Mn^{3+}	640.12	16.66
		641.13	31.43
		643.43	14.54
	Mn^{4+}	642.24	26.24
		644.89	5.42
		646.00	5.70
$Pd/MnO_x/BiVO_4$-after	Mn^{3+}	640.37	5.28
		640.99	30.45
		643.62	16.64
	Mn^{4+}	642.14	37.48
		645.35	5.27
		646.88	4.88

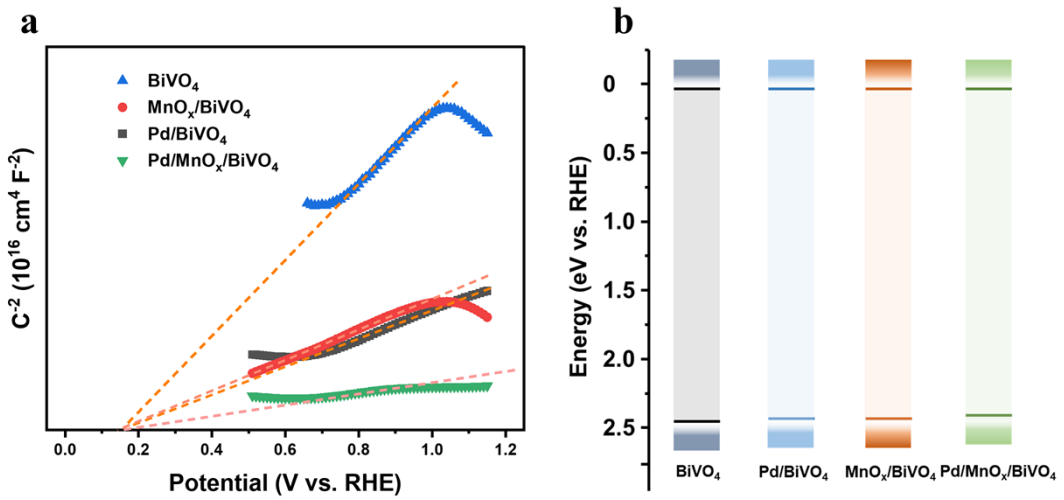

Fig. S17. (a) Mott-Schottky (M-S) measurement for various $BiVO_4$ samples (electrolyte solution: 0.5 M Na_2SO_4). (b) The scheme of band alignment for different $BiVO_4$ samples.

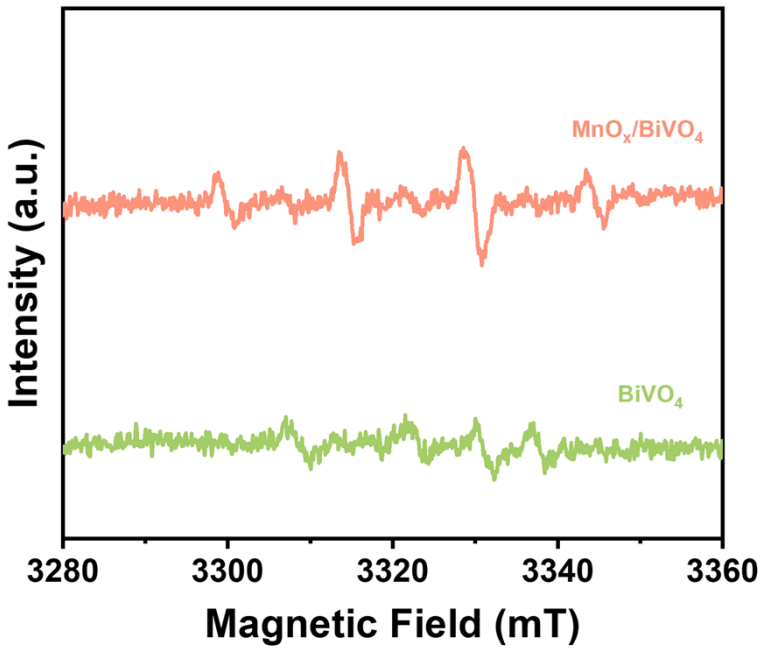

Fig. S18. EPR spectra of DMPO-•OH for $BiVO_4$ and $MnO_x/BiVO_4$ after visible-light irradiation for 1 min.

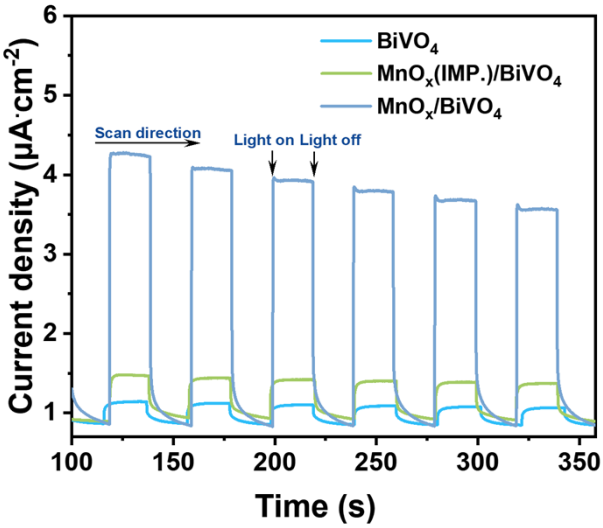

Fig. S19. Photocurrent response curves for $BiVO_4$, MnO_x(imp)/$BiVO_4$ and MnO_x/$BiVO_4$ under chopped illumination (electrolyte solution: 0.5 M Na_2SO_4).

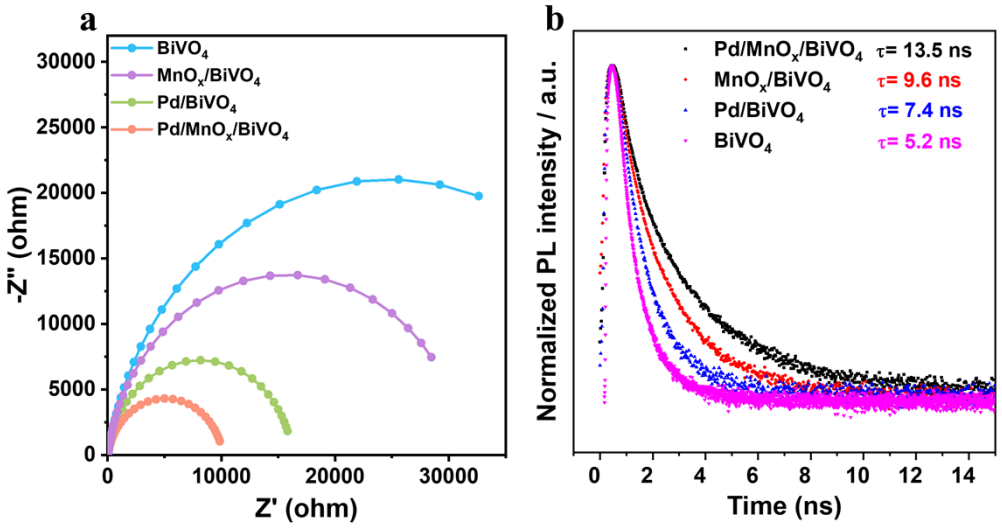

Fig. S20. (a) Photocurrent response curves for r various $BiVO_4$ samples (electrolyte solution: 0.5 M Na_2SO_4). (b) PL decay curves for various $BiVO_4$ samples.

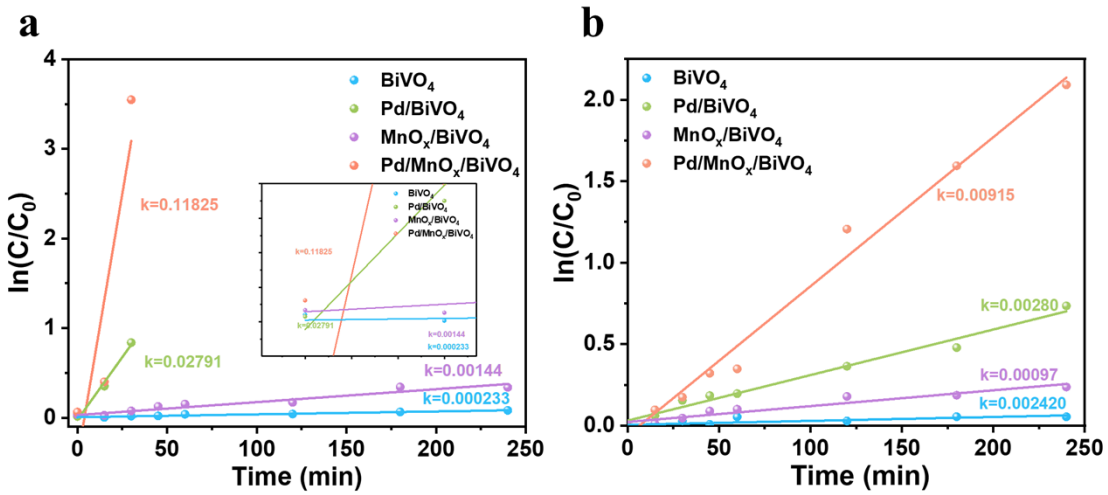

Fig. S21. Kinetic analysis of glyphosate degradation by different $BiVO_4$ samples under continuous gas stream of (a) O_2 and (b) N_2.

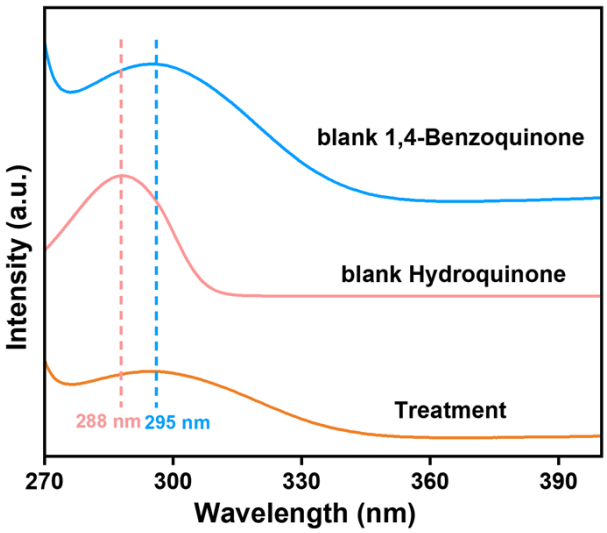

Fig. S22. Reduction experiment of p-Benzoquinone under blank photocatalytic condition.

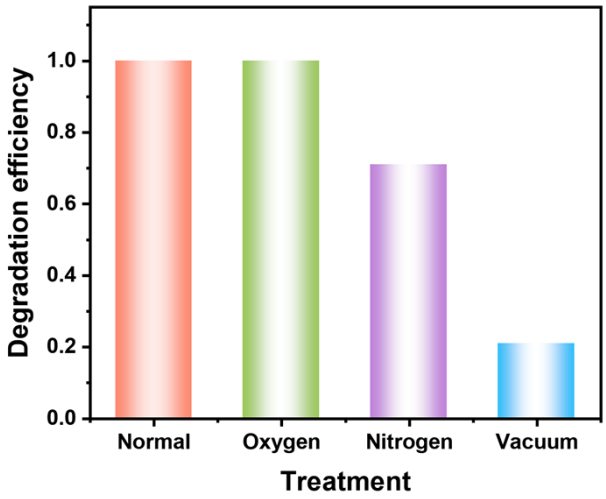

Fig. S23. Glyphosate degradation by $Pd/MnO_x/BiVO_4$ in different atmosphere system for 2 h.

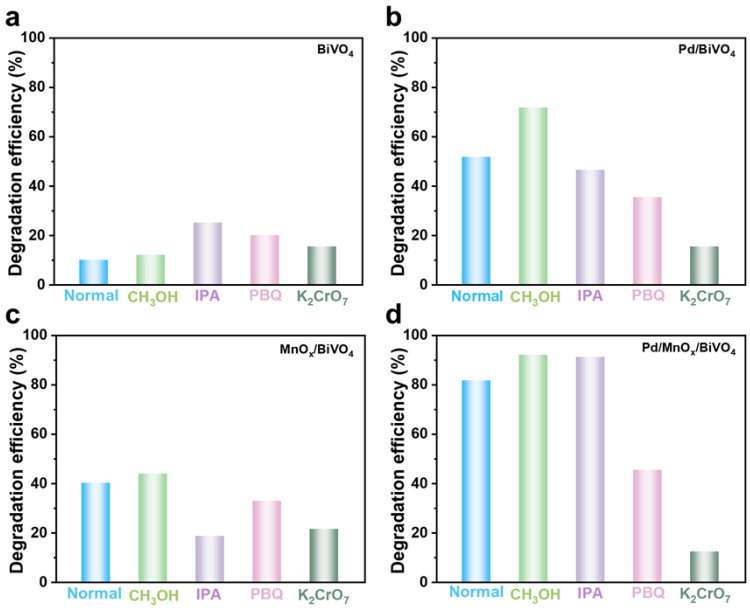

Fig. S24. Normalized degradation efficiencies of glyphosate with the addition of various scavengers by (a) $BiVO_4$, (b) $Pd/BiVO_4$, (c) $MnO_x/BiVO_4$, (d) $Pd/MnO_x/BiVO_4$.

Table S5 Comparison of glyphosate degradation efficiency by different photocatalysts

No.	photocatalyst	Photodegradation efficiency	Degradation time	References
1.	$Pd/MnO_x/BiVO_4$	100%	120 min	This work
2.	$CuO@BiVO_4$	80%	120 min	*Appl. Phys. A* 2023,**129**, 212
3.	$Co(OH)_2$-$BiVO_4$-150	78.3%	30 min	*J. Alloys Compd.* 2024, **976**, 173295.
4.	mCB-MOF-2	69%	24 h	*J.Am.Chem.Soc* 2023, *145,* 25
5.	Sc-TBAPy	100%	150 min	*Nat. Commun.* 2024, **15**, 1459
6.	TiO_2	90%	5 h	*Appl. Catal., B* 2021, **299**, 120671.
7.	TiO_2	100%	120 min	*Chem. Eng. J.* 2019, **360**, 1247-1254